J Mater Sci (2008) 43:378–383
DOI 10.1007/s10853-006-1243-9

Photoacoustic spectra on Mn-doped zinc silicate powders by evacuated sealed silica tube method

Yoshihiro Inoue · Taro Toyoda · Jun Morimoto

Received: 5 December 2005 / Accepted: 10 November 2006 / Published online: 17 October 2007

Abstract The non-radiative transition processes on non-doped Zn_2SiO_4 and Zn_2SiO_4:Mn powders with various Mn concentrations were studied by photoacoustic (PA) spectroscopy. Zn_2SiO_4:Mn_x powders were prepared by dry reaction within an evacuated silica glass tube. As the result of photoluminescence (PL) measurement, the increase of PL intensity for green emission on samples doped with Mn between 1% and 6% and the concentration quenching for luminescence on samples doped with Mn between 7% and 12% were confirmed. For the green luminescence on zinc silicate doped with Mn phosphor, the PL decay behavior is assumed to be due to tunneling directly from excited states of electron traps to the excited states of Mn-ion. The Mn content dependence of PL intensity for green emission is well interpreted by tunneling theory and the results of PA spectra, that is, the green emission is assisted by tunneling from non-radiative levels of Mn-ion to luminescencet level as $^4T_1(^4G)$.

Introduction

Zinc silicate (Zn_2SiO_4) doped with Mn is well known for green phosphor used in plasma display panels [1, 2] because of its high luminescent efficiency and chemical stability. For the preparation of Zn_2SiO_4:Mn_x phosphor, various synthesis methods such as the traditional solid state reaction, sol–gel, hydrothermal, and spray pyrolysis methods are performed [3–7]. Recently, the other Zn_2SiO_4-based phosphors have been investigated for potential in flat panel displays. For example, rare earths such as Eu, Tb and Ce doped Zn_2SiO_4 phosphors can emit red, green and blue light by UV excitation, respectively [8, 9]. Thus, the optimal luminescence properties of Zn_2SiO_4:Mn_x phosphors have been reported extensively [10–15]. In contrast, the details of the non-radiative transition process on Zn_2SiO_4:Mn_x phosphors are hardly reported by evaluation methods such as photoacoustic spectroscopy (PAS) [16]. Here, the PAS can directly evaluate the non-radiative transition process on a sample in contrast to photoluminescence (PL) measurement. The luminescent efficiency is closely related to dopant content, decay time, energy transfer and non-radiative de-excitation process [13]. Hence, it is important to understand non-radiative transition mechanism on phosphors, and the understanding inevitably contributes to improvement of phosphors for the next generation of filed emission displays. PAS with a microphone can enable us to detect acoustic waves generated on a sample surface through heat propagation due to incident light absorption [17], thus we can obtain the information regarding the net light absorption through the non-radiative process. Particularly, PAS is a useful tool for evaluation of powdered samples, which indicate strong light scattering. We have applied PA technique to study the inner state of Pr-ion in ZnO:Pr ceramics powders [18] and the monitoring of a sintering process on ZnO:Co powders, which have internal light scattering [19, 20].

Y. Inoue (✉) · J. Morimoto
Department of Materials Science and Engineering, National Defense Academy, Yokosuka, Kanagawa 239-8686, Japan
e-mail: f05005@nda.ac.jp

T. Toyoda
Department of Applied Physics and Chemistry, The University of Electro-Communications, 1-5-1 Chofugaoka, Chofu, Tokyo 182-8585, Japan

In this study, Zn_2SiO_4:Mn_x powders were prepared by dry reaction within an evacuated silica glass tube, and the luminescence properties were measured by PL and PL excitation (PLE) measurement. Then, we applied PAS to evaluate the non-radiative transition process on non-doped Zn_2SiO_4 and Zn_2SiO_4:Mn powders with various Mn concentrations.

Experimental procedure

The technique of dry reaction within an evacuated silica glass tube is generally used for the synthesis of single crystal for sulfides [21]. We applied this method to prepare Zn_2SiO_4:Mn_x powders, because the dry reaction within the evacuated and closed tube was free from contamination. The starting materials for samples were ZnO powders (99.99%), SiO_2 powders (99.9%), and MnO powders (99.99%) of Kojundo Chemical Lab Co. Ltd. For precursor of mixed powders, ZnO, SiO_2, and MnO powders were weighed as the mole ratio of 66.67–x% : 33.33% : x% adjusted to the stoichiometry of $Zn_{2-0.03x}SiO_4$:$Mn_{0.03x}$, where x was varied between 0 and 12. The weighed powders were mixed in an agate mortar for 1 h. Each of the mixed powders was encapsulated in the evacuated sealed silica glass tube (3.5 mm in diameter and 50 mm in length) with a silica plug, respectively. Here, the tubes and plugs were rinsed ultrasonicly in ethanol and dried. In the capsules, there was hardly remaining free volume. Zn_2SiO_4:Mn_x powders were sintered at 800, 900 and 1000 °C for 24 h with heating and cooling rate of 5 K/min. Crystal phases of samples were characterized by X–ray powder diffraction (XRD) analysis using XRD system (RINT-2200, Rigaku) with Cu K_α radiation accelerated at 40 kV and 40 mA. Luminescent properties of samples were characterized at room temperature by PL and PLE measurements using a Xe lamp as a light source (SPEX Fluorolog-3, Jobin Ybon). Photoacoustic (PA) signals of samples were measured at room temperature using a microphone detector. A 500 W Xe lamp coupled with a monochromator was used as the light source. The excitation light was focused onto the surface of the samples. A microphone and a lock-in amplifier system detected acoustic waves generated above the sample. The incident light was mechanically chopped at 20 Hz. The wavelength of the excitation light was scanned from 350 nm to 650 nm at 1 nm steps. The PA signal intensity was normalized by the PA signals from carbon black to eliminate the effects of the spectral response of the optical apparatus. To determine the background level or noise throughout all experiments, we checked the intensity of the PA signals from carbon black both before and after the measurement.

Results and discussion

Non-doped Zn_2SiO_4

Figure 1 shows the XRD patters of Zn_2SiO_4 powders sintered at 800, 900 and 1000 °C. XRD patterns of samples indicate a rhombohedral structure ($R\bar{3}$) of Zn_2SiO_4 (PDF Card No. 79-2005) in addition to the peaks of SiO_2 phase. For the samples sintered at 800 and 900 °C, the small peaks of ZnO phase are also shown in their XRD patterns, suggesting that the formation of Zn_2SiO_4 is not enhanced below 900 °C of sintering temperature. However, the estimated a-axis length of Zn_2SiO_4 lattice from the peaks of Zn_2SiO_4 in Fig. 1 are almost the same among samples. The peaks of SiO_2 phase are probably attributed to small pieces of SiO_2 film-like mixed in the extracted sample powders. When the sample powders are extracted from the tube, we confirmed pieces of films-like adhered to the internal surface of the silica glass tube. From the analysis by energy dispersive diffraction (EDX) method, the film-like was identified as SiO_2, which was appendant products in sintering process. However, the mixed small pieces of SiO_2 do not affect PL, PLE and PA spectra between measurement wavelength in this study.

As the result of PL measurement, samples showed no visible luminescence except for the weak visible broad luminescence. In particular, the weak visible luminescence

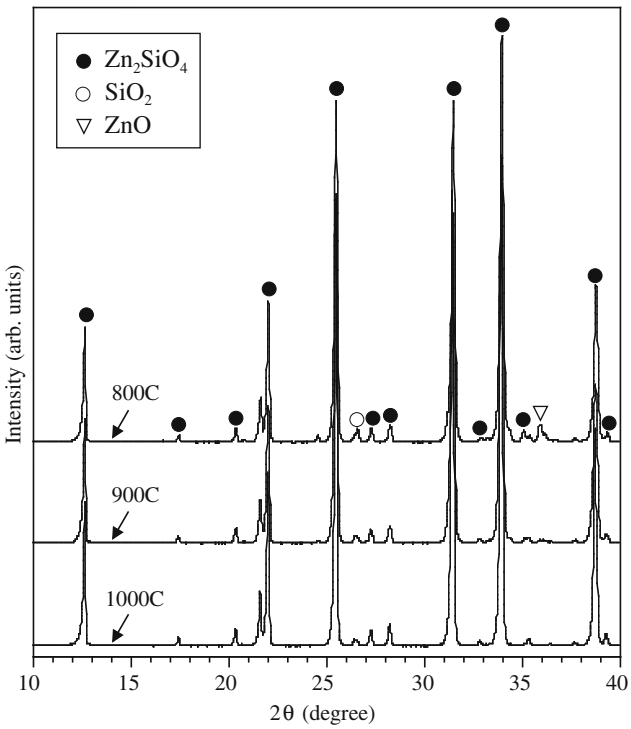

Fig. 1 XRD patters of non-doped Zn_2SiO_4 powders sintered at 800, 900 and 1000 °C

from the sample sintered at 800 °C dominated the weak green broad luminescence centered at about 500 nm, which was probably related to the emission from remained ZnO [22].

PA spectra on Zn_2SiO_4 powders sintered at 800, 900 and 1000 °C are shown in Fig. 2. There is the difference in the change of PA signal intensity between 370 nm and 400 nm, and the flat PA signal are shown in the range between 400 nm and 650 nm. Vanheusden et al. have observed UV fluorescence peaking near 390 nm, obtained with the 232 nm excitation source for ZnO powders [22]. On the other hand, for non-doped Zn_2SiO_4, Hess et al. have observed two PL bands with intensity peaks at 285 and 382 nm in the emission spectra for excitation wavelength of 217 nm, which have been monitored in the PL excitation spectra for 290 nm emission [23]. In Fig. 1, the formation of Zn_2SiO_4 is not enhanced below 900 °C of sintering temperature. Thus, the decrease of PA signal intensity between 350 nm and 400 nm is probably attributed to the emission band of the remained ZnO and/or the synthesized Zn_2SiO_4, it depends on the sintering temperature. This sintering temperature dependence is consistent with the results of XRD analysis and PL measurement for the formation of Zn_2SiO_4 with increasing sintering temperature. While, both the remained ZnO and the synthesized Zn_2SiO_4 have not affected the PA signal between 400 nm and 650 nm. The flat PA spectrum indicates that the non-radiative transitions are not occurred. Hence, we can confirm that there is no levels associated with the remained ZnO and the synthesized Zn_2SiO_4, which cause non-radiative transition, in the range between 400 nm and 650 nm for non-doped Zn_2SiO_4.

Mn doped Zn_2SiO_4

As mentioned above, the formation of Zn_2SiO_4 without remained ZnO phase derived from the dry reaction within an evacuated silica glass tube was achieved at sintering temperature of 1000 °C. Actually, the formation of Zn_2SiO_4:Mn_x(x = 0.03 ~ 0.36) without remained ZnO phase were also achieved at the same sintering temperature as non-doped Zn_2SiO_4 powders. All XRD patters of samples sintered at 1000 °C indicated the same pattern as that of non-doped Zn_2SiO_4 powder sintered at 1000 °C as shown in Fig. 1. As the result of XRD analysis, estimated a-axis lengths of Zn_2SiO_4 lattice on Zn_2SiO_4:Mn samples sintered at 1000 °C were different from that of each other. In Fig. 3, the Mn content dependence of estimated a-axis length of Zn_2SiO_4 lattice is seen. Here, the a-axis lengths tend to increase with increasing Mn content, indicating that the substitution of Mn for Zn are probably allowed up to 12% of Mn content by the dry reaction within an evacuated silica glass tube. The willemite (Zn_2SiO_4:Mn) lattice has two in-equivalent Zn sites (Mn_A and Mn_B) which can influence the radiative decay time, both having nearest neighbor oxygen ions in a slightly distorted tetrahedral configuration [13]. In Fig. 3, it is noticed that there is the variation in a-axis length between 1% and 6% compared with that between 6% and 12%. This probably indicates that the way of being in the two Zn sites for Mn between 1% and 5% is complicated in contrast to that between 6% and 12%.

Typical PL spectra on Zn_2SiO_4:Mn sintered at 1000 °C and the Mn content dependence of PL intensity for green

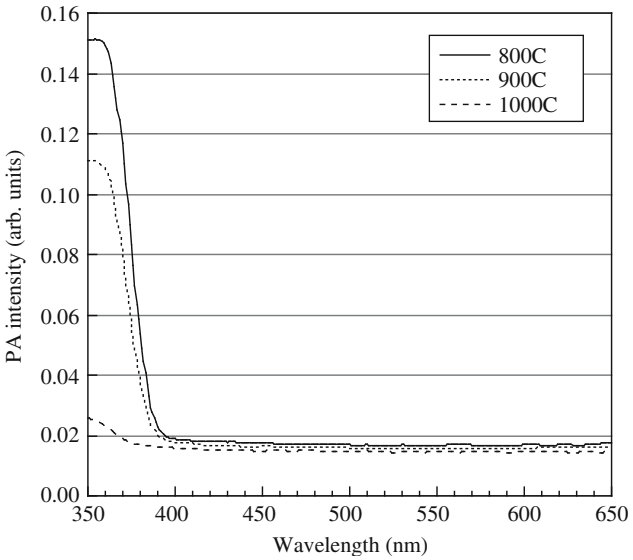

Fig. 2 PA spectra on non-doped Zn_2SiO_4 powders sintered at 800, 900 and 1000 °C

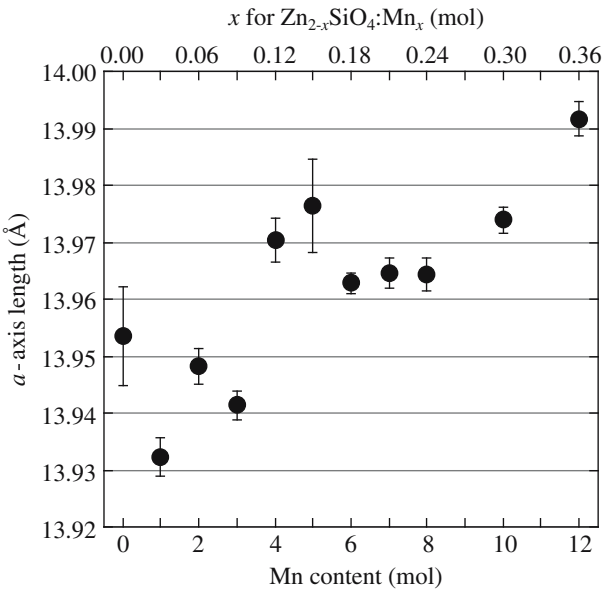

Fig. 3 Mn content dependence of estimated a-axis length of Zn_2SiO_4 lattice for Zn_2SiO_4:Mn powders sintered at 1000 °C

emission peak are shown in Fig. 4a and b, respectively, where the excitation wavelength is 365 nm. The green emission as shown in Fig. 4a are confirmed in all samples, and the origin is attributed to $^4T_1(^4G)$–$^6A_1(^6S)$ transition of Mn-ion [3, 13, 15]. In all samples in this study, the Mn 6% doped Zn_2SiO_4 ($Zn_{1.82}SiO_4$:$Mn_{0.18}$) powders indicates the largest intensity of green emission centered at 527 nm as shown in Fig. 4a and b. Samples doped with Mn over 7% indicate the quenching of luminescence, although Mn atom substitutes for Zn atom up to 12% according to XRD analysis. Sohn et al. studied the concentration quenching on Zn_2SiO_4:Mn_x derived from the solid state reaction, and obtained the critical distance of energy transfer between Mn ions [3]. They estimated the critical distance of 6–9 Å from the calculated spectral overlap data in the case of lower energy excitation, and the estimated value was in good agreement with 10 Å from the concentration quenching data on $Zn_{1.88}SiO_4$:$Mn_{0.12}$ under the excitation wavelength of 254 nm and 423 nm. Comparing their evidence with our results of PL measurement, the quenching of luminescence in Fig. 4b is obviously caused by the concentration quenching, and the critical distance of our sample ($Zn_{1.82}SiO_4$:$Mn_{0.18}$) is presumed to be nearly equal. Furthermore, the wavelength of emission peak shifts from 522 nm to 529 nm between 1% and 12%, where the perpendicular broken line at 527 nm in Fig. 4a is a guide for the eyes. When the Mn concentration increases, the emission band is shifted towards lower energy [13], and that is in agreement with ours. The peak shift between 1% and 6% is larger than that between 6% and 12%. This difference seems to be closely related to the Mn content dependence of *a*-axis length in Fig. 3, that is, the occupation of inequivalent Zn site for Mn. The samples doped with Mn between 1% and 5% have dispersed Mn-ions in random Zn sites in willemite which distort tetrahedral configuration, thus cause the variation in *a*-axis length and the various distance of energy transfer between Mn ions. In contrast, the samples doped with Mn between 7% and 12% have close Mn-ions which cause concentration quenching. In Fig. 5, relative PLE spectra on samples in Fig. 4 monitored at 527 nm are seen. All samples indicate the same spectra with peak A (between 350 nm and 365 nm), B (between 365 nm and 400 nm), C (between 400 nm and 425 nm), D (between 425 nm and 465 nm) and E (between 465 nm and

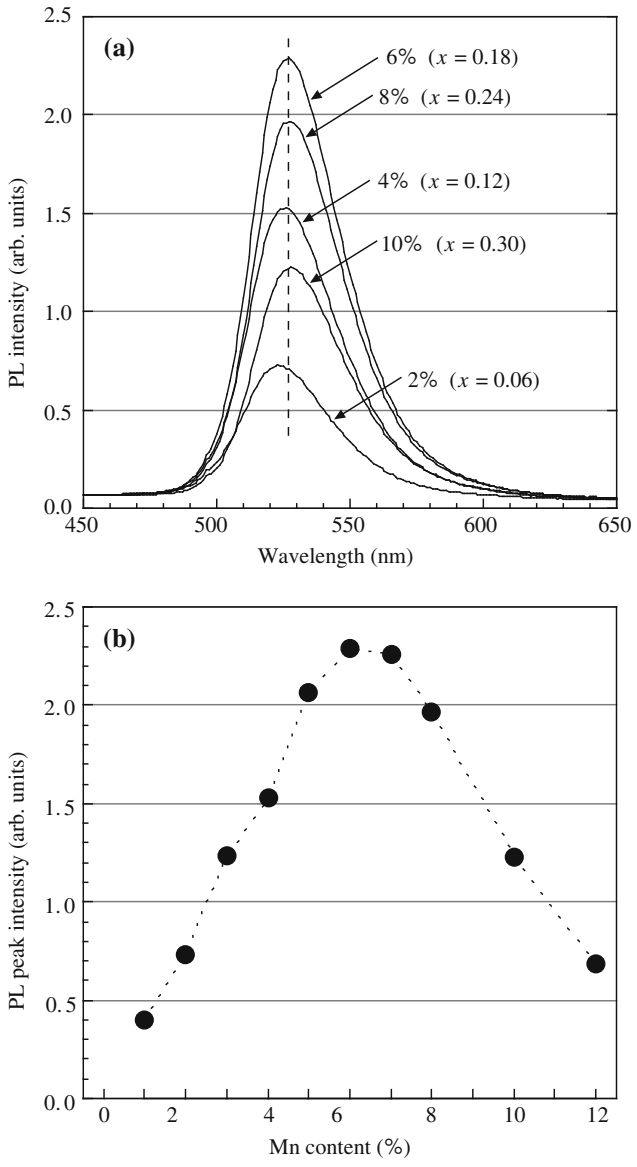

Fig. 4 (**a**) Typical PL spectra on Zn_2SiO_4:Mn sintered at 1000 °C and (**b**) the Mn content dependence of PL intensity for green emission peak, where the excitation wavelength is 365 nm

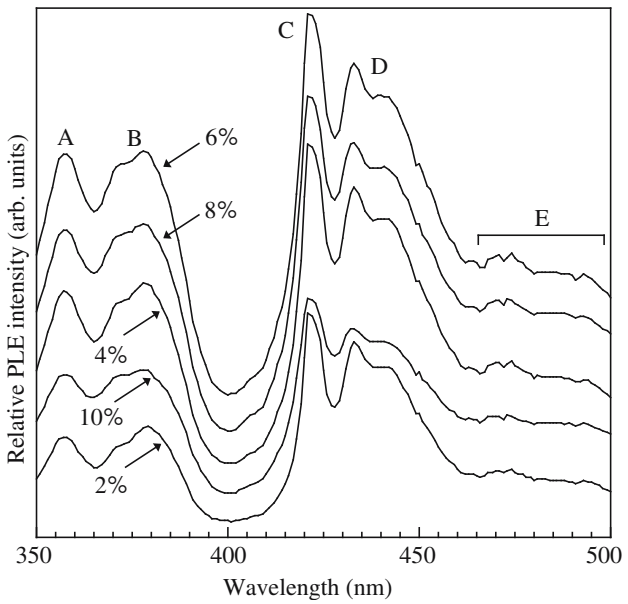

Fig. 5 Typical PLE spectra on Zn_2SiO_4:Mn sintered at 1000 °C, where the monitored wavelength is 527 nm

500 nm), where A, B, C, D and E are attributed to Mn-ion transitions of $^6A_1(S)$–$^4E(^4D)$, $^6A_1(S)$–$^4T_2(^4D)$, $^6A_1(S)$–$^4A_1(^4G)$, $^6A_1(S)$–$^4T_2(^4G)$ and $^6A_1(S)$–$^4T_2(^4G)$ and/or $^4T_1(^4G)$, respectively [3, 15]. Sohn et al. observed the time-resolved excitation spectra of the 524 nm emission on Zn_2SiO_4:Mn phosphor [15]. Our result of PLE measurement corresponds to their result. Additionally, they have observed the absorption edge located at ~4 eV (325 nm), which is assigned to the threshold for the ionization of Mn-ion, in addition to the transition peaks originating in Mn-ion. In our PLE experiment, there is no particular evidence such as the results of XRD analysis and PL measurement in Figs. 3 and 4. Figure 6 shows relative PA spectra on Zn_2SiO_4:Mn powders (Mn: 0, 2, 4, 6, 8, 10 and 12%) sintered at 1000 °C. PA peaks denoted by A, B, C, D and E are appeared with increasing Mn content. These peaks seem to correspond to each PLE peak in Fig. 5 and can be assigned to the light absorption by Mn-ions, suggesting that the Mn-ions contribute to the non-radiative transition center as well as the luminescent center in willemite. PA spectra on the samples of 0, 2, 4 and 6% indicates the flat PA signal between green emission band, however PA spectra on samples of 8, 10 and 12% indicate the PA peak originating in the transition of $^6A_1(S)$ – $^4T_2(^4G)$ and/or $^4T_1(^4G)$ of Mn-ion designated as E. Furthermore, for the samples of 8, 10 and 12%, the PA intensities of non-radiative transitions designated as B, C and D in addition to E become stronger with increasing Mn content. These increases of PA intensity for peaks of B, C, D and E are probably closely related to the concentration quenching as shown in Fig. 4. The sample of 6% indicates maximum green emission of all samples, although the PA spectrum on the sample of 6% indicates PA peaks except for E. This suggests that the levels of Mn-ion originating in PA peaks of A, B, C and D are closely related levels, which are supported by the result of our PLE measurement, for the green emission. For the green luminescence on zinc silicate doped with Mn phosphor, the PL decay behavior is assumed to be due to tunneling directly from excited states of electron traps to the excited states of Mn-ion [10]. The tunneling will take place in a pair if the donor is excited to a tunneling state either by thermal energy or by photon energy, and the Mn doped zinc silicate has four trap levels [24, 25]. Assumed that the green emission is assisted by tunneling from non-radiative levels such as A, B, C and D of Mn-ion to luminescence level as $^4T_1(^4G)$, the increase of PL peak intensity between 1% and 6% and the concentration quenching between 7% and 12% in Fig. 4 are well interpreted. This can be also supported by the Mn content dependence of *a*-axis length in Fig. 3. Zn_2SiO_4-based material is one of ideal materials for flat panel displays. For the improvement of these materials, the investigation about non-radiative transition process is important and required. PAS technique enables us such investigation, in particular, providing that the evaluation of non-radiative transition process on phosphor is useful for an elucidation of luminescent mechanism and quenching caused by activator ions in host material such as zinc silicate.

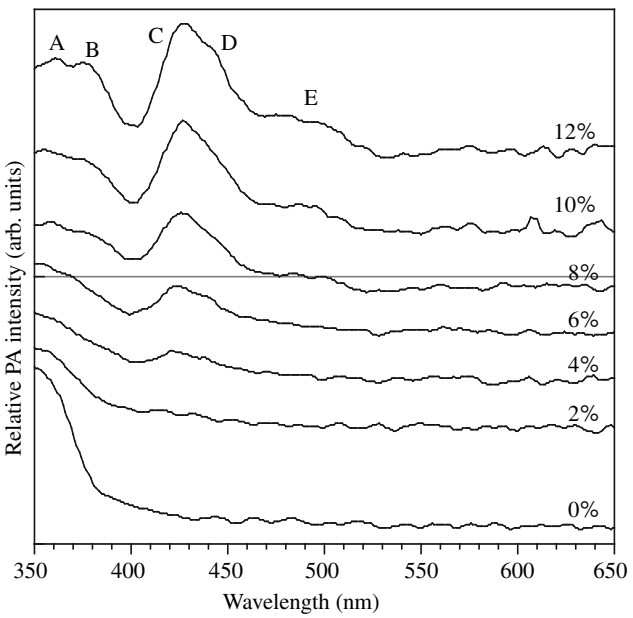

Fig. 6 Typical PA spectra on Zn_2SiO_4:Mn sintered at 1000 °C

Conclusion

Appling PA technique to Zn_2SiO_4:Mn_x powders obtained by dry reaction within an evacuated silica glass tube, we studied the non-radiative transition process on non-doped Zn_2SiO_4 and Zn_2SiO_4:Mn powders with various Mn concentrations. We confirmed the increase of PL intensity for green emission on samples doped with Mn between 1% and 6% and the concentration quenching on samples doped with Mn between 7% and 12%. These evidences are well interpreted by tunneling theory and the results from PA spectra on samples, that is, an assumption that the green emission is assisted by tunneling from non-radiative levels of Mn-ion to luminescence level as $^4T_1(^4G)$.

References

1. Yoon C, Kang S (2001) J Mater Res 16:1210
2. Lee CH, Kang YC, Jung KY, Choi JG (2005) Mater Sci Eng B 117:210
3. Shon K-S, Cho B, Park HD (1999) Mater Lett 41:303
4. Kang YC, Park SB (2000) Mater Res Bull 35:1143
5. Copeland TS, Lee BI, Qi J, Elrod AK (2002) J Lumin 97:168
6. Cho TH, Chang HJ (2003) Ceramics International 29:611

7. Wang H, Ma Y, Yi G, Chen D (2003) Mater Chem Phys 82:414
8. Zhang QY, Pita K, Kam CH (2003) J Phys Chem Solids 64:333
9. Natarajan V, Murthy KVR, Kumar MLJ (2005) Solid State Commun 134:261
10. Chang IF, Thioulouse P, Mendez EE, Giess EA, Dove DB, Takamori T (1981) J Lumin 24/25:313
11. Brownlow JM, Chang IF (1983) IEEE Trans Electron Devices ED-30:479
12. Chang IF, Brownlow JW, Sun TI, Wilson JS (1989) J Electrochem Soc 136:3532
13. Barthou C, Benoit J, Benalloul P (1994) J Electrochem Soc 141:525
14. Li QH, Komarneni S, Roy R (1995) J Mater Sci 30:2358
15. Sohn K-S, Cho B, Park HD (1999) J Am Ceram Soc 82:2779
16. Dove DB, Takamori T, Chang IF, Thioulouse P, Mendez EE, Giess EA (1981) J Lumin 24/25:317
17. Rosencwaig A, Gersho A (1976) J Appl Phys 47:64
18. Inoue Y, Okamoto M, Kawahara T, Morimoto J (2006) J Alloys Compd 408-412:1234
19. Inoue Y, Miyauchi Y, Kimura A, Kawahara T, Okamoto Y, Morimoto J (2004) Jpn J Appl Phys 43:2936
20. . Okamoto M, Inoue Y, Kawahara T, Morimoto J (2005) Jpn J Appl Phys 44:4461
21. Peters TE, Baglio JA (1972) J Electrochem Soc 119:230
22. Vanheusden K, Warren WL, Seager CH, Tallant DR, Voigt JA, Gnade BE (1996) J Appl Phys 79:7983
23. Hess H, Krautz E (1981) J Lumin 24/25:321
24. Yang ES, Brownlow JM (1981) Appl J Phys 52:4753
25. Chang IF, Thioulouse (1982) Appl J Phys 53:5873